SCIENCE CHINA
Technological Sciences

•Article•

May 2018 Vol.61 No.5: 735–747
https://doi.org/10.1007/s11431-017-9151-2

Seismic stability of loess tunnels under the effects of rain seepage and a train load

CHENG XuanSheng[1,2*], MA Liang[1,2], YU DongPo[1,2], FAN Jin[1,2] & LI De[1,2]

[1] *Key Laboratory of Disaster Prevention and Mitigation in Civil Engineering of Gansu Province, Lanzhou University of Technology, Lanzhou 730050, China;*

[2] *Western Engineering Research Center of Disaster Mitigation in Civil Engineering of Ministry of Education, Lanzhou University of Technology, Lanzhou 730050, China*

Received April 6, 2017; accepted September 20, 2017; published online January 11, 2018

Loess tunnels are widely used in transportation engineering and are irreplaceable parts of transportation infrastructure. In this paper, a dynamic finite element method is used to analyze the coupled effects of a train vibration load and rainfall seepage. By calculating the variation in the safety factor of a loess tunnel because of the effects of various factors, such as different rainfall intensities and soil thicknesses, the dynamic stability of the loess tunnel is studied under the condition of a near-field pulse-like earthquake. The results show that the security and stability of the tunnel decrease gradually with decreasing burial depth. In addition, the plastic strain of the tunnel is mainly distributed on both sides of the vault and the feet, and the maximum value of the critical strain occurs on both sides of the arch feet. Because of the effects of the train vibration load and rainfall seepage, the safety factor of the loess tunnel structure decreases to a certain degree. Moreover, the range and maximum value of the plastic strain increase to various degrees.

loess, tunnel, rain water seepage, earthquake, stability

Citation: Cheng X S, Ma L, Yu D P, et al. Seismic stability of loess tunnels under the effects of rain seepage and a train load. Sci China Tech Sci, 2018, 61: 735–747, https://doi.org/10.1007/s11431-017-9151-2

1 Introduction

Economic development has led to the construction of increasing numbers of loess tunnels, providing an indispensable portion of traffic networks. However, macrovoid ratios, vertical joint development and high sensitivity to water make loess tunnels liable to accidents because of the infiltration of underground water and rain water. According to incomplete statistics, during loess tunnel construction, more than 90% of engineering accidents are caused by water seepage [1]. Additionally, the effects of train loads and earthquakes can lead to intense stresses; ultimately, the loess surrounding the tunnel structure can loosen. Low stability under these conditions can cause serious damage to traffic facilities or interrupt transportation. As disasters occur, economic losses and personnel injuries can increase rapidly. Therefore, it is necessary to study the stability of the loess mass surrounding a loess tunnel under the effects of rain water seepage and a train load.

In a railway tunnel, the track structure is subjected to the repeated impact of train loads. Notably, train loads pose a major problem to tunnel operation safety. Over the past century, this issue has attracted increasing attention. Pan and Pande [2] studied the dynamic response of a loess tunnel and presented a similar vibration mode to express the vertical load of a train. Xie et al. [3] discussed the deformation formula of foundation soil caused by different forms of moving loads and compared the effects of different factors on the

*Corresponding author (email: chengxuansheng@gmail.com)

deformation of the soil, such as the moving speed of the train load, the vibration frequency of the load and the track. Bian [4] analyzed the displacement of an observation point in the foundation caused by the impact load generated by a train's response. The authors also examined the dynamic coupling effect of the rail and road pavement. Li et al. [5] analyzed the dynamic response of a train load to a large section tunnel. The stabilities of different section tunnels were also compared under different train speeds and damping ratio coefficients. Zhai et al. [6] obtained displacement, velocity and acceleration time-history curves of a tunnel under a vehicle load. Ye et al. [7] used a layered method to study the dynamic effects of a tunnel under a train load and to analyze the stability of a railway tunnel. Zhang [8] used a simulation model to analyze the vibration response and settlement changes under a metro load in loess strata for the Xi'an Metro system. Wang et al. [9] used the Xi'an subway as an example and employed a numerical analysis method to study the response under a moving subway load. Zheng and Yu [10] analyzed the dynamic response of a subway tunnel to train movement and train vibration. Farhadian et al. [11] used a subregion algorithm to perform three-dimensional coupling calculations for a soil tunnel and analyzed the vibration of the tunnel under a vehicle load. During the construction and operation of a tunnel, it is critical to determine how to implement a seepage prevention system. In engineering, studies of seepage begin with the soil medium. Soil seepage analysis uses seepage theory involving a porous continuous medium. The seepage analysis of a fractured medium begins with single fracture seepage and gradually approaches a complex network system model. Based on closed deformation theory, Liu [12] examined the seepage in a deformable fractured medium under a load in 1987. Anagnostou and Kovári [13] deduced the initial conditions of a tunnel with groundwater in a steady state when the tunnel was excavated. Broere [14] summarized the limiting value of the pore water pressure of a tunnel subjected to underground water effects under conditions in which the stability of the excavation was maintained. Li et al. [15] studied the effects of groundwater on the deformation of a multidimensional tunnel using finite element software. Zhang et al. [16] analyzed the effects of seepage on the stability of a soil slope with a fluctuating water level. Lee et al. [17] used limit equilibrium theory to consider the stability of a soil body under the action of water. Li et al. [18] studied the mathematical formula of the stress and displacement of the mass surrounding a hydraulic tunnel during excavation and seepage. Considering the coupling effect of water and soil in tunnel excavation, Ji et al. [19,20] calculated the displacement and maximum shear stress of the surrounding mass while accounting for seepage. Lee and Nam [21,22] studied the distribution of the surrounding mass of a shallow-buried circular tunnel with underground water during excavation. Li et al. [23] studied the effects of the surrounding mass on the safety of an arch tunnel based on internal and external factors. Li and Zhang [24] applied unsaturated soil flow theory to establish a model of soil and rainfall and used limit equilibrium theory to calculate the slope safety factor. Cheng et al. [25] studied the stability and dynamic response of a submarine tunnel under the effects of temperature and seepage. Liu et al. [26] used a pseudo-static method to analyze the long-term settlement of a saturated soft soil foundation under a subway vibration load. Cheng et al. [27] studied the effect of seepage on the seismic response of a loess tunnel and found that the degree of damage sustained by the loess tunnel because of the combined effects of rainwater seepage and earthquakes was greater than that caused by a single action.

In summary, because of the complexity of the surrounding mass, most scholars have performed static analyses, dynamic analyses and fluid-solid coupled analyses. Based on these studies, this paper considers both a train load and groundwater seepage in using the dynamic finite element static strength reduction method. The safety factor and plastic strain nephogram are obtained, and the dynamic stability of the tunnel structure is analyzed. A comparative study and analysis are performed to demonstrate the importance of considering train load and water seepage, and theoretical support for the analysis of tunnel structure stability is provided.

2 Boundary conditions

An artificial boundary is used to eliminate the effect of the infinite domain [27]. The normal and tangential spring stiffnesses and damping coefficients of the viscoelastic boundary can be determined according to the following formulas:

$$K_{\mathrm{BN}} = \alpha_{\mathrm{N}} \frac{G}{R},\ C_{\mathrm{BN}} = \rho c_{\mathrm{p}}, \tag{1}$$

$$K_{\mathrm{BT}} = \alpha_{\mathrm{T}} \frac{G}{R},\ C_{\mathrm{BT}} = \rho c_{\mathrm{s}}, \tag{2}$$

$$c_{\mathrm{p}} = \sqrt{\frac{E(1-\upsilon)}{\rho(1+\upsilon)(1-2\upsilon)}},\ c_{\mathrm{s}} = \sqrt{\frac{E}{2\rho(1+\upsilon)}}, \tag{3}$$

where K_{BN} is the normal spring stiffness, K_{BT} is the tangential spring stiffness, C_{BN} is the damping coefficient for normal dampers, C_{BT} is the damping coefficient for tangential dampers, R is the distance between the source and the artificial boundary point, c_{p} is the P wave velocity of the medium, c_{s} is the S wave velocity of the medium, α_{N} is the normal viscoelastic boundary correction coefficient, and α_{T} is the tangential viscoelastic boundary correction coefficient. Generally, α_{N} ranges from 0.8 to 1.2 and α_{T} ranges from 0.35 to 0.65. In this paper, α_{N} is 1.0 and α_{T} is 0.5; υ is Poisson's ratio, ρ is the medium density, E is Young's modulus, and G

is shear modulus.

3 Theory of stability analysis

3.1 Theory of soil strength

In general, the linear strength criterion of soil can be expressed by the Mohr-Coulomb yield criterion. The equation can be expressed as follows:

$$f(\sigma,\tau)=\tau=c+\sigma\tan\varphi, \tag{4}$$

where σ is the normal stress on the shear sliding surface, τ is the shear strength of the soil, c is the cohesion of soil, and φ is the internal friction angle of soil.

3.2 Strength reduction method

3.2.1 Modal analysis

In dynamic finite element analyses, the isolated body analysis model typically adopted is the Rayleigh damping matrix model, which assumes that the damping model is related to the mass and stiffness matrix of the structure:

$$\mathbf{C}=\alpha\mathbf{M}+\beta\mathbf{K}, \tag{5}$$

where $\mathbf{C}$ is the damping matrix, $\mathbf{M}$ is the mass matrix, and $\mathbf{K}$ is the stiffness matrix.

According to the orthogonality of the matrix, the coefficients α and β are related to the existence of the viscous damping ratio ζ.

$$\zeta_i=\frac{\alpha}{2f_i}+\frac{\beta f_i}{2}\ (i=1,2,\cdots n), \tag{6}$$

where f_i is the i-th-order frequency.

When ζ is certain, α and β are only related to the natural frequency of the structure. If the one-order and two-order frequencies of the structure can be obtained by the modal analysis, then

$$\begin{cases}\alpha=\dfrac{2f_1f_2\zeta}{f_1+f_2},\\ \beta=\dfrac{2\zeta}{f_1+f_2}.\end{cases} \tag{7}$$

3.2.2 Dynamic equation and its solution

In an earthquake, the differential equation of an isolated body is given as follows:

$$\mathbf{M}\ddot{\mathbf{u}}(t)+\mathbf{C}\dot{\mathbf{u}}(t)+\mathbf{K}\mathbf{u}(t)=-\mathbf{M}\ddot{\mathbf{u}}_{\mathrm{g}}(t)+\mathbf{p}_{\mathrm{f}}, \tag{8}$$

where $\ddot{\mathbf{u}}(t)$ is the acceleration of the model node, $\dot{\mathbf{u}}(t)$ is the velocity of the model node, $\mathbf{u}(t)$ is the displacement of the model node, $\ddot{\mathbf{u}}_{\mathrm{g}}$ is the earthquake acceleration, and $\mathbf{p}_{\mathrm{f}}$ is the vector of the surface load.

The Newmark-β method is used to solve the differential equation matrix:

$$\mathbf{u}_{t+\Delta t}=\mathbf{u}_t+\Delta t\dot{\mathbf{u}}_t+\left(\frac{1}{2}-\varsigma\right)\Delta t^2\ddot{\mathbf{u}}_t+\varsigma\Delta t^2\ddot{\mathbf{u}}_{t+\Delta t}, \tag{9}$$

$$\dot{\mathbf{u}}_{t+\Delta t}=\dot{\mathbf{u}}_t+(1-\imath)\Delta t\ddot{\mathbf{u}}_t+\imath\Delta t\ddot{\mathbf{u}}_{t+\Delta t}, \tag{10}$$

where $\imath$ and ς are constants.

The differential equation of motion at time $t+\Delta t$ is as follows:

$$\mathbf{M}\ddot{\mathbf{u}}_{t+\Delta t}+\mathbf{C}\dot{\mathbf{u}}_{t+\Delta t}+\mathbf{K}\mathbf{u}_{t+\Delta t}=-\mathbf{M}\ddot{\mathbf{u}}_{\mathrm{g}(t+\Delta t)}+\mathbf{P}_{\mathrm{f}}, \tag{11}$$

Regarding the basic parameters of the Newmark-β method, it is reasonable to choose $\imath$=0.5, ς=0.25 and $\Delta t\leqslant T_{\max}/100$ ($T_{\max}$ is the maximum natural vibration period of the model), and the result yields the required accuracy.

Substituting eqs. (9) and (10) into eq. (11) results in the following expression:

$$\left(\mathbf{M}+\frac{\Delta t}{2}\mathbf{C}\right)\ddot{\mathbf{u}}_{t+\Delta t}+\mathbf{C}\left(\dot{\mathbf{u}}_t+\frac{\Delta t}{2}\ddot{\mathbf{u}}_t\right)+\mathbf{K}\mathbf{u}_{t+\Delta t}$$
$$=-\mathbf{M}\ddot{\mathbf{u}}_{\mathrm{g}(t+\Delta t)}+\mathbf{p}_{\mathrm{f}}. \tag{12}$$

From eq. (11), the following equation can be obtained:

$$\ddot{\mathbf{u}}_{t+\Delta t}=\frac{4}{\Delta t^2}(\mathbf{u}_{t+\Delta t}-\mathbf{u}_t)-\frac{4}{\Delta t}\dot{\mathbf{u}}_t-\ddot{\mathbf{u}}_t, \tag{13}$$

Finally, substituting eq. (13) into eq. (12) produces eq. (14):

$$\left(\mathbf{K}+\frac{2}{\Delta t}\mathbf{C}+\frac{4}{\Delta t^2}\mathbf{M}\right)\mathbf{u}_{t+\Delta t}$$
$$=\mathbf{C}\left(\frac{2}{\Delta t}\mathbf{u}_t+\dot{\mathbf{u}}_t\right)+\mathbf{M}\left(\frac{4}{\Delta t^2}\mathbf{u}_t+\frac{4}{\Delta t}\dot{\mathbf{u}}_t+\ddot{\mathbf{u}}_t\right)$$
$$-\mathbf{M}\ddot{\mathbf{u}}_{\mathrm{g}(t+\Delta t)}+\mathbf{p}_{\mathrm{f}}. \tag{14}$$

After eq. (14) is obtained, the displacement vectors in the horizontal and vertical directions can be obtained.

3.2.3 Strength reduction method

The basic concept underlying the strength reduction method is that the shear strength indexes of soil (cohesion c and internal friction angle φ) are divided by a reduction factor η at a certain time, as indicated in eq. (15). After strength reduction, the new shear strength indexes (cohesion c' and internal friction angle φ') are input into the model as the material parameters. The model calculations are performed with the new parameters, and the results are analyzed iteratively until the shear strength parameters are so small that the tunnel reaches the critical failure state. The reduction factor corresponding to the limit equilibrium state is the maximum safety factor of the tunnel.

$$c'=\frac{c}{\eta},\ \phi'=\arctan\left(\frac{\tan\phi}{\eta}\right). \tag{15}$$

Namely,

$$\tau=c'+\sigma\tan\varphi', \tag{16}$$

where c' is the cohesion of the soil after the reduction and φ' is the internal friction angle after the reduction.

3.2.4 Yield criterion

The yield criterion is the point at which a material transitions from an elastic state to a plastic state. In defining the yield condition of rock and soil, the yield of the soil material is related to the hydrostatic pressure. The Mohr-Coulomb yield criterion, which is commonly used for soil, can be expressed as follows:

$$\mathbf{F} = \sqrt{J_2} + \chi I_1 - \lambda = 0, \tag{17}$$

$$J_2 = \frac{1}{6}[(\sigma_1 - \sigma_2) + (\sigma_2 - \sigma_3) + (\sigma_3 - \sigma_1)],$$

$$\chi = \frac{\sin\varphi'}{\sqrt{3(3 + \sin^2\varphi')}},$$

$$\lambda = \frac{3c'\cos\varphi'}{\sqrt{3(3 + \sin^2\varphi')}},$$

where I_1 is the first invariant of the stress tensor, $I_1 = \sigma_1 + \sigma_2 + \sigma_3$, J_2 is the second invariant of the stress tensor.

3.2.5 Failure criterion

The non-convergence criterion is a criterion to judge whether the results are convergent [28] in the process of numerical calculation. Namely, if the result is convergent, the structure is in a stable state; if the results are not convergent, the structure will be an irreversible damage state, at the moment, the factor corresponding to the shear strength reduction is the safety factor of the soil.

3.2.6 Calculation progress

In this paper, a dynamic finite element static strength reduction analysis of the stability of a tunnel structure is performed [29]. This approach is a dynamic structural analysis based on a model, in which the analysis results are input into the static model. The cohesion and angle of internal friction of the loess mass surrounding the tunnel are then decreased. By reducing the shear strength parameters of the loess mass until the model does not converge, the safety factors of the loess mass can be obtained. This process is implemented as follows. First, the structural analysis model is established. Then, a modal analysis is carried out to investigate the natural frequency of the structure. Next, a dynamic analysis is performed, and the Rayleigh damping coefficients are used to obtain the boundary horizontal displacement, the maximum horizontal displacement of the model top [30]. Then, static strength reduction is performed. In the static analysis model, the horizontal displacement values are the initial displacements applied to corresponding nodes on the boundaries. Finally, by using the shear strength parameters to continuously reduce the internal friction angle and cohesion of the loess mass, the safety factor of the loess mass associated with the tunnel is obtained.

4 Seepage theory of a loess mass under train vibrations

4.1 Summary

Assuming that the vibration due to train load is vertical, and that the ultimate equilibrium condition of the soil under static state is the same as that under dynamic state, and that the damage envelope line about Mohr-Coulomb under the static load is the same as that under the dynamic load, the dynamic and static effective internal friction angles of the soil are the same [31].

Figure 1 shows the stress circle before the train vibration and the stress circle of the dynamic stress amplitude σ_{do} during train operation. Expansion or contraction of the soil occurs under the drainage condition, which causes the development of excess pore water pressure [32]. Because of the repeated vibration of the train load, the tunnel foundation soil is subjected to repeated shearing actions, which alter the configuration state of the soil mass and the physical and mechanical properties of the soil. In addition, the high-speed and short-duration train vibrations caused by poor drainage condition in a high pore water pressure. After many repetitions, the residual pore water pressure will gradually increase, the effective stress will decrease, and the stress circle will move to the failure surface until damage occurs in the medium.

As shown in Figure 1, when the accumulated pore water pressure reaches the critical value of 0, the corresponding vibration load will lead to the loss of soil mass. Before the train occurs to vibration, the surrounding pressure force τ does not generate shear stress. When σ increases, the soil becomes denser, and the pore water pressure decreases. Under the action of dynamic load, the accumulated pore water pressure increases as the cycle number and stress amplitude increase. In isotropic consolidation, the pore water pressure formula of SETRA-Fenn is as follows:

$$\frac{u}{\sigma_3} = \frac{2}{\pi}\sin^{-1}\left(\frac{N}{N_f}\right)^{\frac{1}{\theta}}, \tag{18}$$

where u is the pore water pressure accumulated over N cycles, N_f is the number of vibrations based on the dynamic stress amplitude-driven strength curve, and θ is a parameter based on the soil properties, species and density.

K_c is the consolidation stress ratio of the soil, where $K_c = \frac{\sigma_1}{\sigma_3}$ indicates the consolidation degree of the soil in a natural state.

When K_c>1, the formula can be expressed as follows:

$$\frac{u}{\sigma_3} = \frac{1}{2} + \frac{2}{\pi}\sin^{-1}\left[\delta\left(\frac{N}{N_{50}}\right)^{\frac{1}{\theta}} - 1\right], \tag{19}$$

where N_{50}, as illustrated by the pore water pressure development curve, indicates the corresponding cycle of $u = 0.5\sigma_3$.

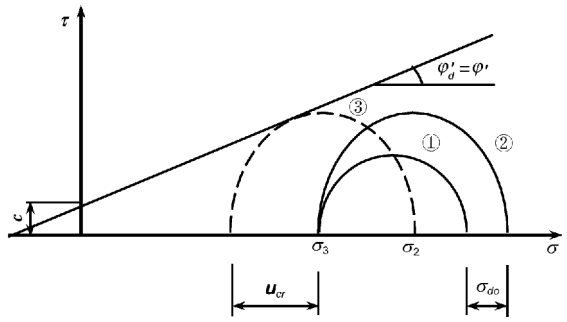

Figure 1 Mohr-Coulomb failure curve under dynamic loading.

δ is a soil parameter with a general value of 1.0, θ is related to the consolidation stress ratio of K_c soil parameters and can be expressed as $\theta = \alpha_1 K_c + \alpha_2$. Among these parameters, α_1 and α_2 are experimentally measured.

4.2 Mathematical model of porous media seepage field

4.2.1 Seepage rate

According to Darcy's law [33]:

$$\begin{cases} v_1 = -\dfrac{k}{\iota'}\left(\dfrac{\partial p}{\partial x} + \rho g \sin\psi\right), \\ K = k\dfrac{\gamma}{\iota'}, \end{cases} \tag{20}$$

where v_1 is the flow velocity of the liquid, ι' is viscosity, p is the Cauchy pore pressure, ψ is the angle between the velocity direction and the horizontal plane, k is permeability, γ is bulk density, and K is the permeability coefficient.

4.2.2 Equilibrium equation

According to the literature [34], the equilibrium equations with displacement and pore water pressure as the basic unknown quantities are

$$\begin{cases} \dfrac{\mu}{(1-2\upsilon)}\dfrac{\partial \varepsilon_v}{\partial x} + \mu \nabla^2 W_x + n\dfrac{\partial p}{\partial x} = 0, \\ \dfrac{\mu}{(1-2\upsilon)}\dfrac{\partial \varepsilon_v}{\partial y} + \mu \nabla^2 W_y + n\dfrac{\partial p}{\partial y} = 0, \\ \dfrac{\mu}{(1-2\upsilon)}\dfrac{\partial \varepsilon_v}{\partial z} + \mu \nabla^2 W_z + n\dfrac{\partial p}{\partial z} + \\ \left[(1-n)\rho_s + n\rho_w\right]\cdot g_z = 0, \end{cases} \tag{21}$$

where W_x, W_y and W_z are the displacements of the solid skeleton in the x-, y- and z-directions respectively, n is porosity, ε_v is volume strain, $\varepsilon_v = \dfrac{\partial W_x}{\partial x} + \dfrac{\partial W_y}{\partial y} + \dfrac{\partial W_z}{\partial z}$, and μ is the Lame constant.

4.2.3 Seepage control equation

According to the literature [35]:

$$\tilde{V} = -K \cdot (\nabla p), \tag{22}$$

where $\tilde{V}$ is relative velocity.

Assuming that a saturated porous medium is in single-phase flow, the control equation of the porous medium skeleton is [34]

$$\nabla \cdot \left[\rho_s (1-n)\vec{V}_s\right] + \frac{\partial\left[\rho_s(1-n)\right]}{\partial t} = 0, \tag{23}$$

where $\vec{V}_s$ is the absolute velocity of skeleton particles.

According to the literature [36], the fluid in the pores should satisfy the following formula:

$$\nabla^{\mathrm{T}} \cdot (-K \cdot \nabla p) = \frac{\partial \varepsilon_{ii}}{\partial t} + \frac{n}{E_w}\frac{\partial p}{\partial t}, \tag{24}$$

and

$$\begin{cases} \dfrac{1}{\rho_w}\dfrac{\partial \rho_w}{\partial t} = \dfrac{1}{E_w}\dfrac{\partial p}{\partial t}, \\ \dfrac{1}{\rho_s}\dfrac{\partial \rho_s}{\partial t} = \dfrac{1}{E_s}\dfrac{\partial p}{\partial t}, \end{cases} \tag{25}$$

where ε_{ii} is the Cauchy strain, E_w is the compression modulus of the water, E_s is the compression modulus of the soil skeleton.

According to eqs. (22)–(25), the mass equilibrium equation of saturated porous media, which is the fluid-solid coupling seepage equation of porous media, can be obtained [37].

$$\left(\frac{n}{E_w} + \frac{1-n}{E_s}\right)\frac{\partial p}{\partial t} + \frac{\partial \varepsilon_{ii}}{\partial t} + \nabla^{\mathrm{T}} \cdot (-K \cdot \nabla p) = 0. \tag{26}$$

The mathematical model of fluid-solid coupling seepage is composed of eq. (21) and eqs. (23), (24) or (26).

4.3 Seepage equation of a loess mass under train vibrations

Assuming that the soil is an isotropic porous medium composed of solids and fluids, soil seepage obeys Darcy's law, the soil is incompressible, rigid displacement and deformation will occur, and the viscous coupling force due to the soil motion is given as follows.

Solid phase:

$$\sigma_{ij,j} + R_i = (1-n)\rho_s \ddot{u}_i, \tag{27}$$

Liquid phase:

$$\sigma_j + R_i = n\rho_w \ddot{U}_i, \tag{28}$$

where $\sigma_{ij,j}$ is the solid-phase pressure per unit area, σ_j is the pore fluid pressure per unit area, R_i is the viscous force of the liquid relative to the solid phase, $\ddot{u}_i$ and $\ddot{U}_i$ are the displacement components of the solid phase and liquid phase, respectively, ρ_s is the mass density of the solid phase, and ρ_w is the mass density of the liquid phase.

Darcy's law can be expressed in the x-direction as follows:

$$Q = \frac{K_x A(h_1 - h_2)}{L}, \tag{29}$$

where Q is the volumetric flow through the porous medium per unit time, A is the cross-sectional area, h_1 and h_2 are the initial water height and end water height respectively, L is the length of the sample, and K_x is the permeability coefficient. The gravitational potential energy of water head is substituted into eq. (29) as follows:

$$\frac{Q}{A}=\frac{K_x\left(p'_1-p'_2\right)}{\rho_{\mathrm{w}}gL}, \tag{30}$$

where p'_1 and p'_2 are the water pressures at the initial water height and end water height, respectively.

When L tends to zero and $\frac{Q}{A}=n(\dot{U}_x-\dot{u}_x)$, the formula can be expressed as

$$\frac{\partial p'}{\partial x}=\frac{n\rho_{\mathrm{w}}g}{K_x}\left(\dot{U}_x-\dot{u}_x\right), \tag{31}$$

where p' is water pressure.

The left part of the formula is the resistance of the fluid to the skeleton, and the pressure is positive. The average per unit area is given as follows:

$$R_x=n\frac{\partial p'}{\partial x}=n^2\frac{\rho_{\mathrm{w}}g}{K_x}\left(\dot{U}_x-\dot{u}_x\right). \tag{32}$$

If k_x is taken as the permeability in the x-direction, $\frac{\rho_{\mathrm{w}}g}{K_x}=\frac{1}{k_x}$, eq. (32) can be rewritten as follows:

$$R_x=\frac{n^2}{k_x}\left(\dot{U}_x-\dot{u}_x\right). \tag{33}$$

Similarly, the viscous force in the y-direction is given as follows:

$$R_y=\frac{n^2}{k_y}\left(\dot{U}_y-\dot{u}_y\right). \tag{34}$$

If $b_x=\frac{n^2}{k_x}$ and $b_y=\frac{n^2}{k_y}$, eqs. (33) and (34) can be substituted into eqs. (27) and (28). Based on the result and the principles of effective stress, namely, $\sigma_{ij}=\sigma'_{ij}+(1-n)\sigma_{\mathrm{w}}$ and $\sigma=n\sigma_{\mathrm{w}}$ (σ_{ij} and σ'_{ij} are the total stress and effective stress respectively), the following equations can be established.

The differential equation of solid-phase motion is as follows:

$$\begin{cases}\dfrac{\partial\sigma_x}{\partial x}+\dfrac{\partial\tau}{\partial y}+(1-n)\dfrac{\partial\sigma_{\mathrm{w}}}{\partial x}+b_x\left(\dfrac{\partial v_x}{\partial t}-\dfrac{\partial u_x}{\partial t}\right)\\ =(1-n)\rho_{\mathrm{s}}\dfrac{\partial^2u_x}{\partial t^2},\\ \dfrac{\partial\sigma_y}{\partial y}+\dfrac{\partial\tau}{\partial x}+(1-n)\dfrac{\partial\sigma_{\mathrm{w}}}{\partial y}+b_y\left(\dfrac{\partial v_y}{\partial t}-\dfrac{\partial u_y}{\partial t}\right)\\ =(1-n)\rho_{\mathrm{s}}\dfrac{\partial^2u_y}{\partial t^2}.\end{cases} \tag{35}$$

Additionally, the differential equation of liquid-phase motion is as follows:

$$\begin{cases}n\dfrac{\partial\sigma_{\mathrm{w}}}{\partial x}+b_x\left(\dfrac{\partial v_x}{\partial t}-\dfrac{\partial u_x}{\partial t}\right)=n\rho_{\mathrm{w}}\dfrac{\partial^2u_x}{\partial t^2},\\ n\dfrac{\partial\sigma_{\mathrm{w}}}{\partial y}+b_y\left(\dfrac{\partial v_y}{\partial t}-\dfrac{\partial u_y}{\partial t}\right)=(1-n)\rho_{\mathrm{w}}\dfrac{\partial^2u_y}{\partial t^2}.\end{cases} \tag{36}$$

In eqs. (35) and (36), u_x is the displacement of the soil skeleton in the x-direction, u_y is the displacement of the soil skeleton in the y-direction, v_x is the displacement of water in the x-direction, v_y is the displacement of water in the y-direction, ρ_{s} is the density of the soil, ρ_{w} is the density of water, b_x is the permeability coefficient of damping in the x-direction, b_y is the permeability coefficient of damping in the y-direction, σ_x is the effective stress in the x-direction, σ_y is the effective stress in the y-direction, σ_{w} is the pore water pressure, and τ is the shear stress.

In addition, based on the compressibility of the two phases in the saturated porous medium, the volumetric compression modulus of the liquid phase is as follows:

$$E_{\mathrm{w}}=-\rho_{\mathrm{w}}\frac{\mathrm{d}\sigma_{\mathrm{w}}}{\mathrm{d}\rho_{\mathrm{w}}}. \tag{37}$$

Additionally, the bulk compressive modulus of solid particles is given as follows:

$$E_{\mathrm{s}}=-\rho_{\mathrm{s}}\frac{\mathrm{d}\left(\frac{\Theta^{\mathrm{s}}}{1-n}\right)}{\mathrm{d}\rho_{\mathrm{s}}}. \tag{38}$$

Moreover, $\frac{\Theta^{\mathrm{s}}}{1-n}=\frac{\sum\sigma_{ii}^{\mathrm{s}}}{3(1-n)}=\frac{\sum\sigma_{ii}}{3(1-n)}+\sigma_{\mathrm{w}}=\frac{\Theta}{1-n}+\sigma_{\mathrm{w}}$, $\Theta=\frac{\sum\sigma_{ii}}{3}$ is the average solid effective stress. The following formula can be obtained by consolidating the solid phase and liquid phase in the equation of state.

$$\begin{cases}-\dfrac{\mathrm{d}\rho_{\mathrm{s}}}{\rho_{\mathrm{s}}}=\dfrac{\mathrm{d}\Theta}{E_{\mathrm{s}}(1-n)},\\ \dfrac{\mathrm{d}\rho_{\mathrm{w}}}{\rho_{\mathrm{w}}}=-\dfrac{\mathrm{d}\sigma_{\mathrm{w}}}{E_{\mathrm{w}}}.\end{cases} \tag{39}$$

In a two-phase medium, if the mutual transformation between two phases is not considered, the law of mass conservation yields the following equations.

Solid phase:

$$\frac{\partial}{\partial t}\left[(1-n)\rho_{\mathrm{s}}\right]+div\left[\rho_{\mathrm{s}}(1-n)\dot{\mathbf{u}}\right]=0; \tag{40}$$

Liquid phase:

$$\frac{\partial}{\partial t}(n\rho_{\mathrm{w}})+div\left(\rho_{\mathrm{w}}n\dot{\mathbf{v}}\right)=0. \tag{41}$$

According to these formulas, expanding eqs. (40) and (41) and ignoring negligible variables yields the following expressions.

$$(1-n)div\dot{\mathbf{u}}+\frac{1-n}{\rho_{\mathrm{s}}}\frac{\partial\rho_{\mathrm{s}}}{\partial t}=\frac{\partial n}{\partial t}, \tag{42}$$

$$ndiv\dot{\mathbf{v}} + \frac{n}{\rho_w}\frac{\partial \rho_w}{\partial t} = \frac{\partial n}{\partial t}. \tag{43}$$

Adding these two formulas yields eq. (44):

$$(1-n)div\dot{\mathbf{u}} + div\dot{\mathbf{v}} + \frac{1-n}{\rho_s}\frac{\partial \rho_s}{\partial t} + \frac{n}{\rho_w}\frac{\partial \rho_w}{\partial t} = 0. \tag{44}$$

In addition, inserting eq. (43) into eq. (44) yields the following formula.

$$(1-n)div\dot{\mathbf{u}} + ndiv\dot{\mathbf{v}} - \frac{1}{E_s}\frac{\partial((1-n)\sigma_w + \Theta)}{\partial t} - \frac{n}{E_w}\frac{\partial \sigma_w}{\partial t} = 0. \tag{45}$$

Under typical conditions, the soil medium is incompressible; thus, the compatibility equation of the two phases is as follows:

$$(1-n)div\dot{\mathbf{u}} + ndiv\dot{\mathbf{v}} - \frac{n}{E_w}\frac{\partial \sigma_w}{\partial t} = 0, \tag{46}$$

or

$$\sigma_w = \frac{1-n}{n}E_w div\mathbf{u} + E_w div\mathbf{v}. \tag{47}$$

Based on the relationship between strain and displacement and assuming that the pore fluid is a theoretical fluid, the relationship between displacement and strain is as follows:

$$\begin{cases} e_{ij} = \dfrac{1}{2}\left(\dfrac{\partial u_i}{\partial x_j} + \dfrac{\partial u_j}{\partial x_i}\right), \\ \overline{\varepsilon}_{ii} = e_{ij} = div\mathbf{u}, \\ \overline{\varepsilon}_v = div\mathbf{v}. \end{cases} \tag{48}$$

Eq. (46) can be written in the following form, namely, the continuity equation:

$$n\frac{\partial \overline{\varepsilon}_v}{\partial t} + (1-n)\frac{\partial \overline{\varepsilon}_u}{\partial t} = \frac{n}{E_w}\frac{\partial \sigma_w}{\partial t}, \tag{49}$$

where $\overline{\varepsilon}_v$ is the compressive strain of the water, and $\overline{\varepsilon}_u$ is the strain of the soil skeleton.

5 Seismic stability of a loess tunnel under the effects of rain water seepage and a train load

5.1 Calculation parameters

In this paper, when the structural analysis model is established, the loess mass grade of the tunnel is grade IV, and the lining structure of the tunnel is established as a composite concrete lining. The loess mass of the tunnel is defined as a Mohr-Coulomb material, and the concrete lining around the tunnel is defined as an elastic-plastic material. The damping ratio of the lining of the tunnel is 0.05, and the damping ratio of the loess mass of the tunnel is 0.35 [38]. Concrete parameters are shown in Table 1. Loess parameters before and after rainfall are shown in Table 2.

Because of the impact of vertical and horizontal rail forces, the bottom of the loess railway tunnel is directly under a train load; therefore, the track structure must be sufficiently strong and stable. The structure and material parameters of the ballast bed are directly related to the stability and safety of the train. A single ballastless track bed is used in the concrete of the tunnel, and the track width is 1.045 m. The end of the track is filled with concrete whose strength is 25 MPa. The foundation and the track plate use 300 mm- and 150 mm-thick concrete elastic-plastic material, respectively; the physical parameters of the concrete materials are shown in Table 3.

5.2 Seismic wave

Velocity pulses are most common in near-field earthquakes, which exhibit a waveform similar to that of pulses and feature long duration. Moreover, middle-period and long-period components are abundant, and the pulse peak is large. According to the characteristics of seismic waves, the selection principle, the hypocenter type and the hypocentral distance, a near-field seismic wave with pulses is selected from the Pacific Earthquake Engineering Research Center, and the acceleration magnitude of the seismic wave is adjusted to satisfy the requirements of seismic fortification under the rare earthquake. According to the duration characteristic and period of seismic waves, the duration of the seismic wave is selected to be 15 s, and the seismic acceleration time-history curve is shown in Figure 2. The seismic load is input in the form of acceleration at the model boundary.

5.3 Train load

For the train load [39], the vertical force is reduced to a

Table 1 Concrete parameters

Material type	Elastic modulus (GPa)	Poisson's ratio	Unit weight (kN/m^3)	Cohesion (MPa)
Initial lining	30	0.2	25	–
Secondary lining	30	0.2	25	–

Table 2 Loess parameters

Type	Elastic modulus (MPa)	Poisson's ratio	Unit weight (kN/m^3)	Cohesion (MPa)	Internal friction angle (°)
Before the rain	85	0.35	18.5	0.1	25
After the rain	30	0.35	15.58	0.075	19.8

Table 3 The material parameters of track bed

Material types	Elastic modulus (MPa)	Poisson′s ratio	Unit weight (kN/m^3)
Filling material at the bottom of the tunnel	17.5	0.2	18
Concrete foundation	30	0.2	25
Track slab	30	0.2	25

moving point load $P(t)$, which is varies time, that is

$$P(t) = k_1 k_2 \begin{bmatrix} p_0 + p_1 \sin(\omega_1 t) + p_2 \sin(\omega_2 t) \\ + p_3 \sin(\omega_3 t) \end{bmatrix}, \quad (50)$$

where p_0 is the train static load, p_1, p_2 and p_3 are typical values of the vibration load under control conditions involving ride stability, dynamic additional load on the lines and wave abrasion respectively, k_1 is the superposition coefficient of the adjacent wheel-rail force, which is typically 1.2–1.7, and k_2 is the wheel-rail dispersion coefficient, which is typically 0.6–0.9.

Assuming that the unsprung mass of the train is M_0, the corresponding vibration load amplitude is

$$P_i = M_0 a_i \omega_i^2 \ (i = 1, 2, 3), \quad (51)$$

where a_i represents typical values of the vibration load under control conditions involving ride stability, dynamic additional load on the lines and wave abrasion, respectively; and ω_i is the vibration circle frequency of the irregularity control condition, $\omega_i = 2\pi \frac{v_2}{L_i}$ (v_2 is train speed, L_i is the typical wavelength of the geometric irregularity curve).

The axle load of a train is directly related to the railway design grade, and different countries have different standards and codes. The most commonly used reference range for the train axle load is 15–17 t, except in China. In China, the first ten-thousand-ton train with a 30 t axle load is already in use, but for the practicability of the research results, in this paper, the train axle load is taken as 22 t, which is commonly used in China. Unsprung mass M_0 is 750 kg. Based on China's high-speed railway operation standards and the irregular vibration wavelength and arch rise [40], v_2=300 km/h, L_1= 10 m, L_2=2 m, L_3=0.5 m, a_1=3.5 mm, a_2=0.4 mm, and a_3=0.08 mm. Thus, the low-frequency, medium-frequency and high-frequency ranges of the train load at speeds of 180–324 km/h are 5–9, 25–45 and 100–200 Hz, respectively, consistent with the test data obtained from the UK Railway Research Center. The train load time-history curve at a speed v_2=300 km/h is shown in Figure 3.

5.4 Analysis model

Through preliminary analysis, the maximum response of the tunnel due to earthquake generally occurs about the moment 8–10 s, therefore, the train load is applied after the moment 7 s. As shown in Figure 3, the duration time of the train load is 4 s (namely, from the moment of 7 s to 11 s). The force of gravity on the train is applied to the model in the form of a dead load, and the train load is applied to the model by defining the load time history. Based on the train load, two points are selected as the action positions of the load, and the time-history curve of the simulation is applied at the two points. The thickness of the soil overlying the loess tunnel is 30 m.

The seepage field has a direct effect on the stress field through the seepage volume force, while the stress field acts indirectly on the seepage field by changing the volume strain. Through the interaction between the seepage field and the stress field, double-field coupling can reach a relatively balanced and stable state. The seepage field and stress field are then gradually stabilized under the effects of one another. In the finite element program, the direct coupling method is adopted to solve the control equations of the coupling field. Loess is defined as a porous continuous medium to account for the elastoplastic deformation of the soil skeleton, and the seepage flow is analyzed by defining the fluid control

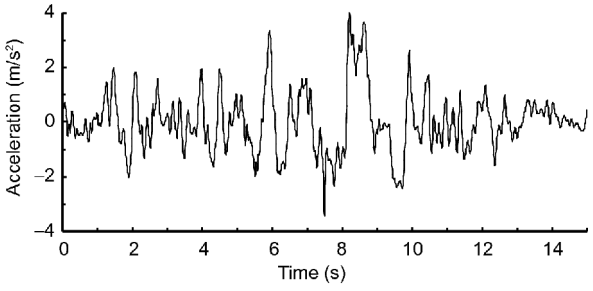

Figure 2 Acceleration time-history curve of 8 degree rare earthquake (near-field earthquake with pulses).

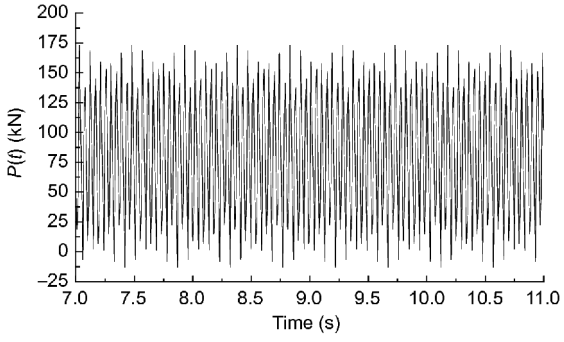

Figure 3 Train load time-history curve.

equation in the medium by mean velocity and seepage rate; the seepage can then be simulated. During seepage in a porous continuous medium, the pore pressure is altered by structural deformation. The stress field of the fluid affects the physical and mechanical parameters of the porous continuous medium. Herein, the permeability is 3×10^{-10}, the porosity is 0.0005, and the viscosity is 0.001. The analysis model is shown in Figure 4.

Based on the seepage theory outlined in Section 4, the seepage control equations and boundary conditions are transformed into an extreme value problem of the universal function, and the region studied is divided into finite elements. The local equations of the elements are established by a continuous piecewise interpolating function, and all the elements are assembled through the relations among nodes. Therefore, the system of linear algebraic equations is solved.

5.5 Seismic stability under the effects of moderate rain and a train load

Considering earthquake effects, the near-field pulse seismic wave that has the strongest influence on structural safety is used in the analysis. The acceleration time-history curve in the horizontal direction of the model is shown in Figure 2. The thicknesses of the soil layer overlying the tunnel are 30, 60 and 80 m; the rainfall intensity is 30 mm/d; and the rain water penetrates 1 m below the Earth's surface [41]. Using the dynamic finite element static strength reduction method, the horizontal displacement time-history curves at node 818 (the right vertex of the model) are shown in Figure 5.

The maximum horizontal displacements at node 818 are obtained from the model at 10.67, 11.91 and 12.10 s. The corresponding horizontal displacement values of each node are then derived at the same moments in the dynamic model on the left and right boundaries. Then, the derived displacement values are applied to each node on the left and right boundaries of the static analysis model. The shear strength parameters of the loess mass are continuously reduced, and the plastic strain nephograms of the loess mass of the tunnel under different overlying loess thicknesses are shown in Figure 6.

Figure 6 shows the effects of both the train vibration load and rainwater seepage, and the safety factor of the loess tunnel can be determined from these figures based on different overlying loess thicknesses. The safety factor of a deep buried tunnel is greater than that of a shallow buried tunnel. Additionally, the stability of a deep buried tunnel is higher than that of a shallow buried tunnel. The plastic strain of the tunnel is mainly distributed on both sides of the vault and the arch feet. The maximum value is located at the arch feet, which indicates that the safety and stability of the tunnel decline as the tunnel depth decreases.

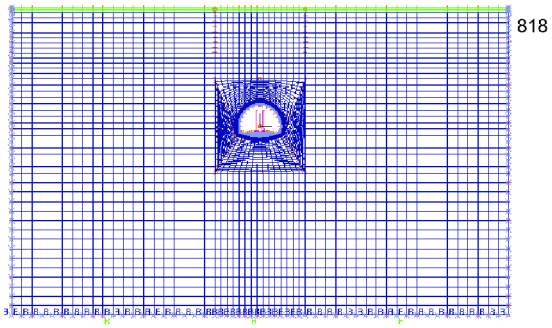

Figure 4 (Color online) Analysis model.

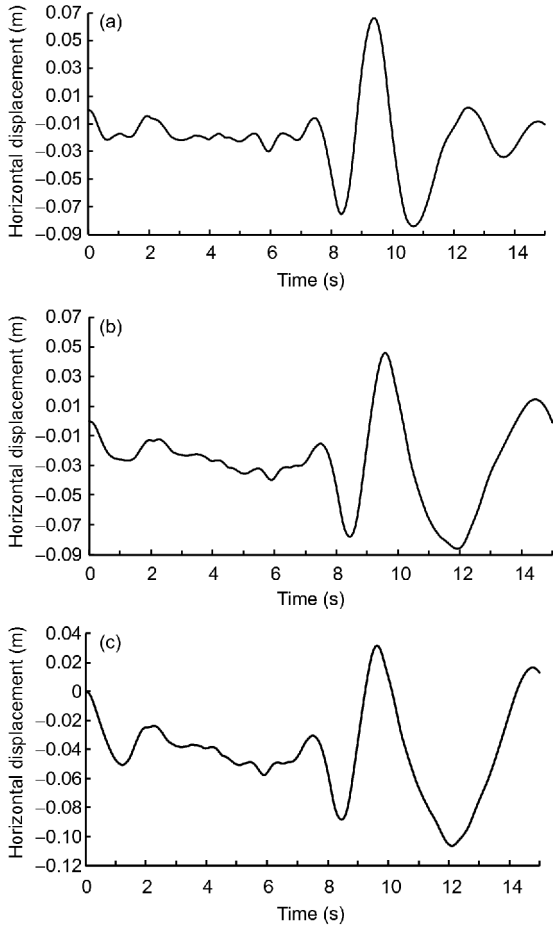

Figure 5 Horizontal displacement time-history curves at node 818. (a)–(c) The overlying loess thicknesses are 30, 60 and 80 m, respectively.

5.6 Seismic stability under the effects of heavy rain and a train load

In the case of heavy rain, the rainfall intensity is set to 65 mm/d, the rain infiltration depth is 1.5 m, and the overlying loess thickness is 30, 60 or 80 m. The horizontal displacement curves at node 818 are shown in Figure 7.

The time-history curves of the horizontal displacement and

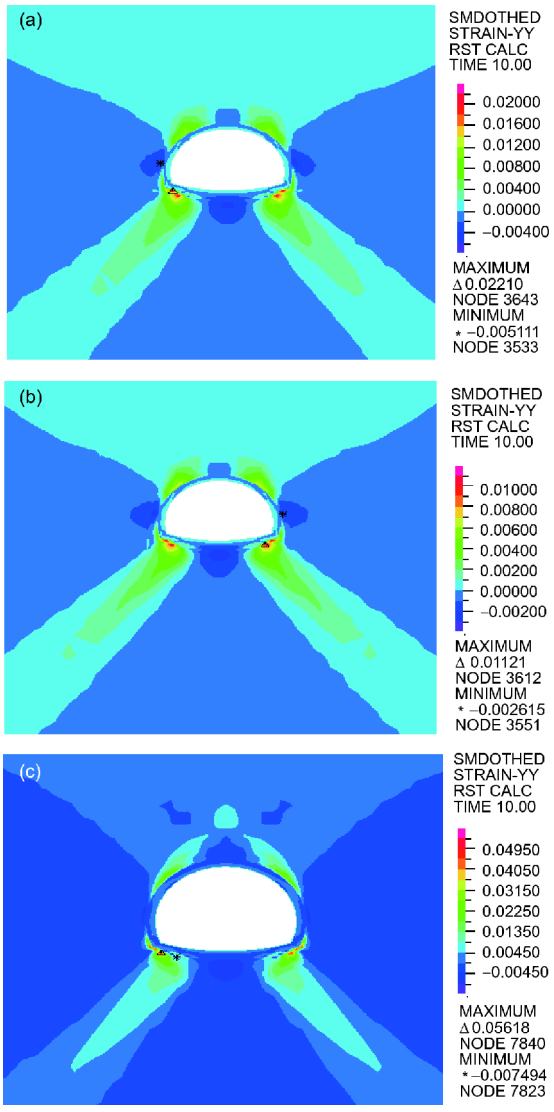

Figure 6 (Color online) Plastic strain nephogram of the loess mass of the tunnel for overlying loess thicknesses of 30 (a), 60 (b) and 80 m (c). The safety factors of the tunnels are 2.253 (a), 2.273 (b) and 2.654 (c).

the extreme values shows that the maximum displacement of the model occurs at 10.67, 11.91 and 12.10 s. The horizontal displacement of each node at the left and right boundaries is then derived from these values. The displacement values obtained are applied to the static analysis model of the corresponding nodes, and the shear strength parameters of the loess mass are considered. Finally, the effects of heavy rain and a train load on the critical plastic strain of the loess tunnel are shown in Figure 8 for different overlying loess thicknesses.

Figure 8 shows that in the case of a train load and heavy rain, the safety factor of the tunnel is 2.250 for a loess thickness of 30 m, 2.265 for a loess thickness of 60 m and 2.647 for a loess thickness of 80 m. The critical plastic strain nephogram shows that the plastic strain of the tunnel is mainly distributed around the vault and the arch feet, with the

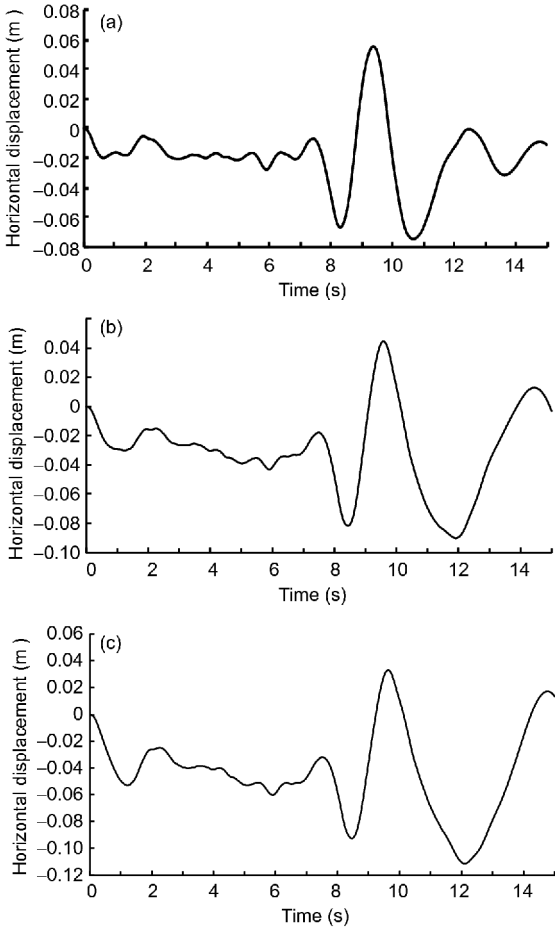

Figure 7 Horizontal displacement time-history curves of the right apex of the tunnel. (a)–(c) The overlying loess thicknesses are 30, 60 and 80 m, respectively.

maximum value of the critical strain occurring on both sides of the arch feet. Moreover, the safety and stability of the tunnel increase as the burial depth increases.

5.7 Seismic stability based on the effects of a train load and rainstorm

In this case, the rainfall intensity is 75 mm/d, the infiltration depth of rainwater is 2 m, and the thickness of the overlying loess layer is 30, 60 or 80 m. A near-field seismic wave pulse is used, the dynamic analysis models are adopted using different overlying thicknesses to determine the horizontal displacement at node 818, as shown in Figure 9.

The horizontal displacement curves in Figure 9 show that the maximum horizontal displacements at node 818 are at 10.67, 11.91 and 12.10 s for different overlying thicknesses. The horizontal displacement of the moment is input into the static analysis model of the tunnel for different overlying loess thicknesses, and the shear strength parameters of the loess mass are continuously reduced. The plastic strain results are shown in Figure 10.

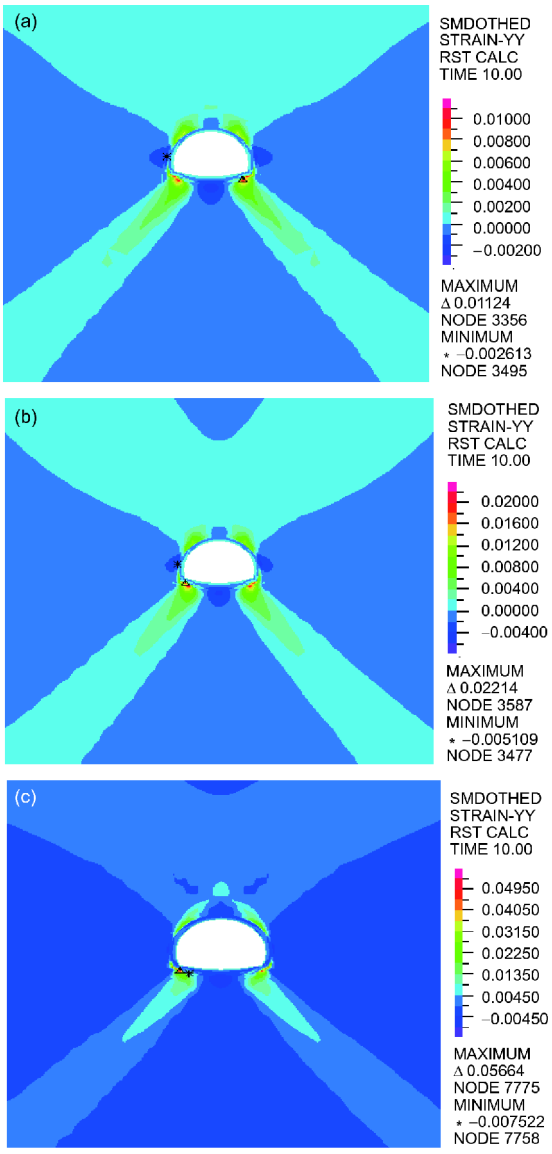

Figure 8 (Color online) Plastic strain nephogram of the loess mass for overlying loess thicknesses of 30 (a), 60 (b) and 80 m (c). The safety factors of the tunnels are 2.250 (a), 2.265 (b), and 2.647 (c) respectively.

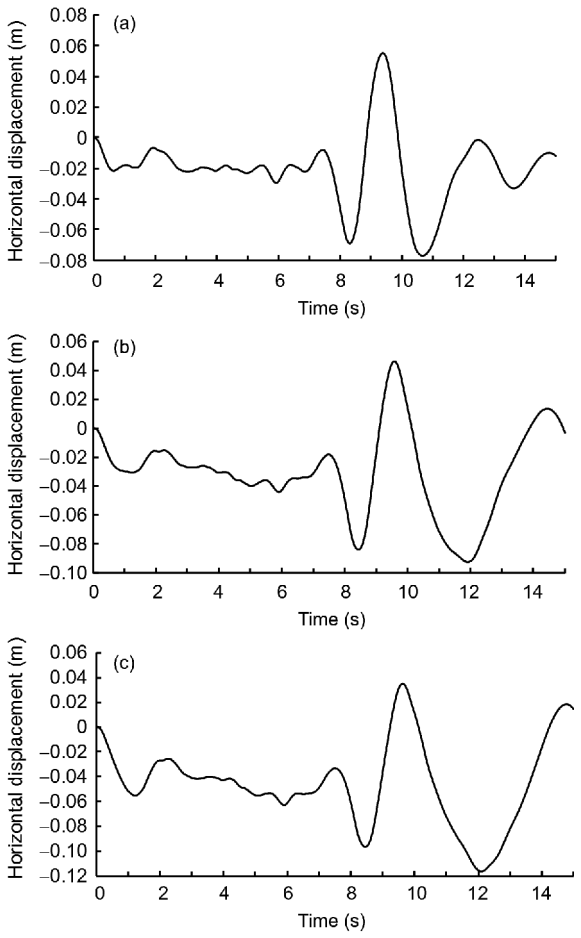

Figure 9 Horizontal displacement time-history curves at node 818. (a)–(c) The overlying loess thicknesses are 30, 60 and 80 m, respectively.

In the case of the train vibration load, the safety factor of the loess mass of the tunnel is relatively constant at different overlying loess thickness under the condition of critical failure, as shown in Figure 10. Moreover, as the buried depth increases, the safety factor of the tunnel increases, which indicates that the stability factor increases with burial depth. The plastic strain nephograms show that plastic strain mainly occurs on both sides of the tunnel vault and the arch feet, and the maximum strain on both sides of the lower arch waist gradually extends to the arch feet. Thus, the safety and stability of the tunnel decrease with decreasing depth.

Based on the abovementioned analysis of the factors that affect the stability of the tunnel, the safety factor of the tunnel under the combined effects of a train load and different rainfall intensities is determined, as shown in Figure 11.

Figure 11 shows that the safety factor of the loess mass of the tunnel increases as the buried depth increases and declines as the rainfall intensity increases. For overlying soil thicknesses of 30, 60 and 80 m and different rainfall intensities, water seepage decreases by approximately 0.443%–0.662%, 0.044%–0.220% and 0.711%–0.863%, respectively, compared with the values obtained under conditions without rain. The numerical analysis results show that the liquefaction of the soil is accelerated by the vibration of the train and the effect of fluid seepage. Therefore, for tunnels with buried depths of 30, 60 and 80 m, in the case of moderate rain, the safety factors increase from 2.253 to 2.273 and then to 2.654, respectively. In the case of heavy rain, the safety factors increase from 2.250 to 2.265 and then to 2.647, respectively. Moreover, in the case of a rainstorm, the safety factors of the tunnel increase from 2.248 to 2.260 and then to 2.641, respectively.

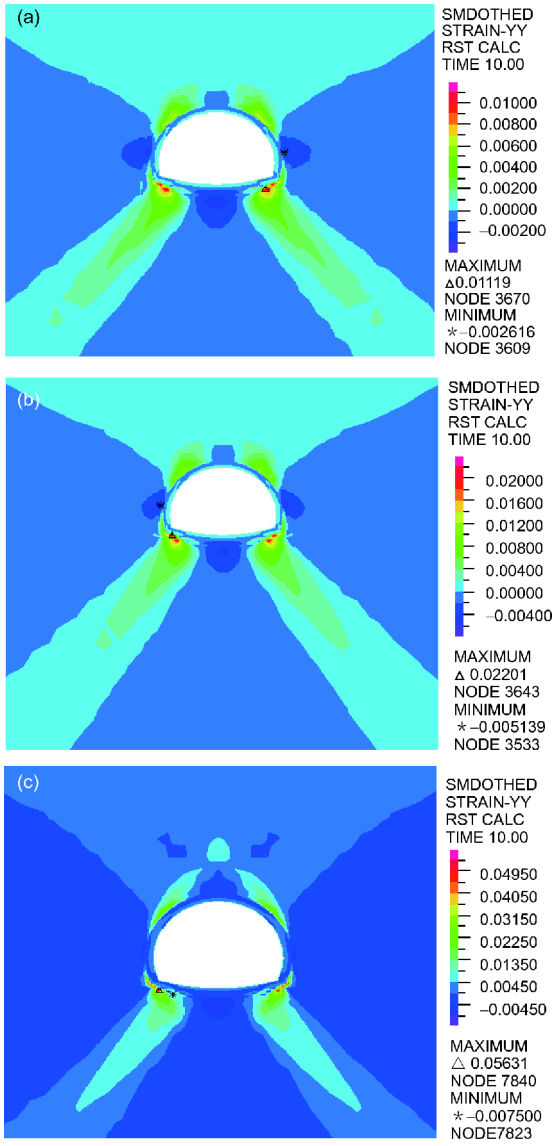

Figure 10 (Color online) Plastic strain nephogram of the loess mass of a tunnel for overlying loess thicknesses of 30 (a), 60 (b) and 80 m (c). The safety factors of the tunnels are 2.248 (a), 2.260 (b) and 2.641 (c).

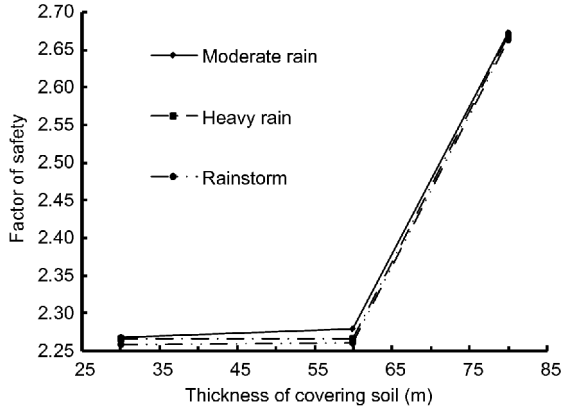

Figure 11 Safety factor of the loess tunnel for a train load and different rainfall intensities.

6 Conclusions

When rain water seepage, a train vibration load and a near-field impulse earthquake occur simultaneously (for the same rainfall intensity and overburden thickness), the safety factor of the loess mass of the tunnel is reduced to a certain extent. Additionally, the range and maximum value of plastic strain increase to various degrees.

When rain water seepage, a train vibration load and a near-field impulse earthquake occur simultaneously, for the same rainfall intensity, the safety factor changes slightly when the overlying soil thickness is less than 60 m. However, when the overlying soil thickness is greater than 60 m, the safety factor increases remarkably.

When rain water seepage, a train vibration load and a near-field impulse earthquake occur simultaneously, for the same overlying thickness, the effect of rainfall intensity on the safety factor is very small, namely, the rainfall intensity and the safety factor are not discernibly related.

This work was supported in part by the National Natural Science Foundation of China (Grant No. 51478212) and the Education Ministry Doctoral Tutor Foundation of China (Grant No. 20136201110003).

1 Xian D Q. Analysis of main causes of foundation engineering accidents (in Chinese). Mineral Explor, 2004, 7: 11–13
2 Pan C S, Pande G N. Analysis of dynamic load response of loess tunnel by finite element method (in Chinese). China Civil Eng J, 1984: 21–30
3 Xie W P, Wang G B, Yu Y L. Calculation of soil deformation caused by moving load (in Chinese). Chin J Geotech Eng, 2004, 2: 318–322
4 Bian X C. Dynamic response analysis of foundation and tunnel under moving load of high speed train (in Chinese). Dissertation of Doctoral Degree. Zhejiang: Zhejiang University, 2005
5 Li L, Zhang B Q, Yang X L. Dynamic response analysis of large section tunnel under vibration load of high speed train (in Chinese). Chin J Rock Mech Eng, 2005, 24: 4259–4265
6 Zhai L H, Shi H O, Jiang P P. Analysis of soil dynamic response and impact of high speed railway vibration load on metro tunnel (in Chinese). Urban Mass Transit, 2012, 15: 32–37
7 Ye F, Ding W Q, Wang G B, et.al. Study on the influence of train moving load on stability of down road tunnel (in Chinese). Rock Soil Mech, 2008, 29: 549–552
8 Zhang K. Vibration response and settlement of loess stratum under subway driving load (in Chinese). Dissertation of Doctoral Degree. Xi'an: Xi'an University of Architecture and Technology, 2011
9 Wang X, Han X, Zhou H L. Study of the numerical calculation of ground response under metro traffic loading in a loess area. Mod Tunneling Technol, 2014, 51: 152–160
10 Zheng J, Yu S F. Dynamic responses of underground structures generated by high-speed train loads (in Chinese). Struct Eng, 2013, 29: 46–50
11 Farhadian H, Aalianvari A, Katibeh H. Optimization of analytical equations of groundwater seepage into tunnels: A case study of Amirkabir tunnel. J Geol Soc India, 2012, 80: 96–100
12 Liu J S. Seepage formula of a fracture subject to normal stress (in Chinese). Hydrol Eng Geol, 1987: 36–37
13 Anagnostou G, Kovári K. Face stability conditions with earth-pressure-balanced shields. Tunn Undergr Space Tech, 1996, 11: 165–173
14 Broere W. Face stability calculation for a slurry shield in heterogeneous soft soils. In: Negro Jr A, Ferreira A A, Eds. Tunnels and

Metropolises. Netherlands: A.A. Balkema Publishers, 1998. 215–227
15 Li X, Zhang W, Li D, et al. Influence of underground water seepage flow on surrounding rock deformation of multi-arch tunnel. J Cent South Univ Technol, 2008, 15: 69–74
16 Zhang W J, Chen Y M, Ling D S. Seepage and stability analysis of bank slopes (in Chinese). J Hydraul Eng, 2005, 36: 1510–1516
17 Lee I M, Nam S W, Ahn J H. Effect of seepage forces on tunnel face stability. Can Geotech J, 2003, 40: 342–350
18 Li Z L, Ren Q W, Wang Y H. Elasto-plastic analytical solution of deep-buried circle tunnel considering fluid flow field (in Chinese). Chin J Rock Mech Eng, 2004, 23: 1291–1295
19 Ji X M, Wang Y H. Hydraulic coupling analysis of tunnel excavation process (in Chinese). Chin J Undergr Space Eng, 2005, 1: 848–852
20 Ji X M. Discussion on the research of coupled solid and fluid flow in tunnel engineering (in Chinese). Chin J Undergr Space Eng, 2006, 2: 149–154
21 Lee I M, Nam S W. The study of seepage forces acting on the tunnel lining and tunnel face in shallow tunnels. Tunn Undergr Space Tech, 2001, 16: 31–40
22 Lee I M, Nam S W. Effect of tunnel advance rate on seepage forces acting on the underwater tunnel face. Tunn Undergr Space Tech, 2004, 19: 273–281
23 Li D Y, Li X B, Zhang W, et al. Stability analysis of surrounding rock of multi arch tunnel based on fluid structure interaction theory (in Chinese). Chin J Rock Mech Eng, 2007, 26: 1056–1064
24 Li Z P, Zhang M. Study on transient safety factor of unsaturated soil slope considering rainfall infiltration (in Chinese). China Civil Eng J, 2001, 34: 57–60
25 Cheng X, Dowding C H, Tian R. New methods of safety evaluation for rock/soil mass surrounding tunnel under earthquake. J Cent South Univ, 2014, 21: 2935–2943
26 Liu M, Huang M S, Li J J. Long term settlement analysis of saturated soft clay under subway load (in Chinese). Chin J Undergr Space Eng, 2006, 2: 813–817
27 Cheng X, Feng H, Qi S, et al. Dynamic response of curved wall LTSLS under the interaction of rainwater seepage and earthquake. Geotech Geol Eng, 2017, 35: 903–914
28 Zheng Y R, Zhao S Y. Application of strength reduction FEM in soil and rock slope (in Chinese). Chin J Rock Mech Eng, 2004, 23: 3381–3388
29 Cheng X S, Zheng Y R, Tian R R. Dynamic finite element strength reduction method of earthquake stability analysis of surrounding rock of tunnel (in Chinese). Rock Soil Mech, 2011, 32: 1241–1248
30 Cheng X S, Zheng Y R. Calculation discussion about safety factor of unlined loess tunnel wall rock structure under earthquake (in Chinese). Rock Soil Mech, 2011, 32: 761–766
31 Xie W P, Sun H G. FEM analysis on wave propagation in soils induced by high speed train loads (in Chinese). Chin J Rock Mech Eng, 2003, 22: 1180–1184
32 Chen Z Y, Zhou J X, Wang H J. Soil Mechanics. Beijing: Tsinghua University Press, 2002
33 Wang T H, Luo Y, Zhang H. Two-dimensional steady flow rate equation for loess joints (in Chinese). Chin J Geotech Eng, 2013, 35: 1115–1120
34 Li P C, Kong X Y, Lu D T. Mathematical modeling of flow in saturated porous media on account of fluid-structure coupling effect (in Chinese). J Hydrodyn, 2003, 18: 419–426
35 Yuan L J, Li Z S, Wu S Z, et al. Engineering Seepage Mechanics and Its Application. Beijing: China Building Materials Press, 2001
36 ADINA R & D, Inc. ADINA Theory and Modeling Guide, Volume I: ADINA Solids & Structures. Watertown MA, 2010. 559–561
37 Wang X, Wang L B. Dynamic analysis of a water-soil-pore water coupling system. Comp Struct, 2007, 85: 1020–1031
38 Hu Z Y, Luo Y S, Li Y. Experimental study on damping ratio variation characteristics of loess in different areas (in Chinese). Earthq Eng Eng Vib, 2010, 30: 167–172
39 Chen L, Chen G X, Li L M. Seismic response characteristics of the double-layer vertical overlapping metro tunnels under near-field and far-field ground motions (in Chinese). China Railw Sci, 2010, 31: 79–86
40 Cui Y X, Bi Z Q, Gong Q M. Dynamic analysis of ballastless track-subgrade considering frequency-dependent subgrade equivalent parameters (in Chinese). China Sciencepaper, 2015, 10: 745–749
41 Su H J, Liu Z Z, Huang Z H, et al. A model test investigation on infiltration depth of soil slope under sustained rainfall (in Chinese). China Sci Paper, 2015, 10: 91–94